Eclipse-induced wind changes over the British Isles on the 20 March 2015

Article

Accepted Version

PHILOSOPHICAL TRANSACTIONS A

rsta.royalsocietypublishing.org

Research

Article submitted to journal

Subject Areas:

xxxxx, xxxxx, xxxx

Keywords:

meteorology, eclipse, measurements, nocturnal jet

Author for correspondence:

S. L. Gray

e-mail: s.l.gray@reading.ac.uk

Eclipse-induced wind changes over the British Isles on the 20 March 2015

S. L. Gray[1] and R. G. Harrison[1]

[1] Department of Meteorology, University of Reading, P.O. Box 243, Reading, RG6 6BB, U.K.

The British Isles benefits from dense meteorological observation networks, enabling insights into the still-unresolved effects of solar eclipse events on the near-surface wind field. The near-surface effects of the solar eclipse of 20 March 2015 are derived through comparison of output from the Met Office's operational weather forecast model (which is ignorant of the eclipse) with data from two meteorological networks: the Met Office's land surface station (MIDAS) network and a roadside measurement network operated by Vaisala. Synoptic-evolution relative calculations reveal the cooling and increase in relative humidity almost universally attributed to eclipse events. In addition, a slackening of wind speeds by up to about 2 knots in already weak winds and backing in wind direction of about 20° under clear skies across middle England are attributed to the eclipse event. The slackening of wind speed is consistent with the previously reported boundary layer stabilisation during eclipse events. Wind direction changes have previously been attributed to a large-scale 'eclipse-induced cold-cored cyclone', mountain slope flows, and changes in the strength of sea breezes. A new explanation is proposed here by analogy with nocturnal wind changes at sunset and shown to predict direction changes consistent with those observed.

THE ROYAL SOCIETY PUBLISHING

1. Introduction

Solar eclipse events cause a unique natural perturbation to the Earth's atmospheric system. After the effects on solar radiation, humankind perceives solar eclipses most obviously through their effects on the near-surface atmospheric conditions: namely temperature, relative humidity (RH), and wind speed and direction. Beyond their importance as a scientific curiosity of nature, these changes can give rise to socio-economic impacts. For example, an eclipse in Svalbard led to the formation of fog that grounded air traffic [1] and the reduction of solar radiation and commonly observed reduction in near-surface wind speeds can both negatively impact the generation of renewable energy. The cooling and increases in RH attributable to eclipses are well documented. In contrast, there is less consensus on induced changes in circulation. The purpose of this study is to investigate the meteorological responses to the solar eclipse of 20 March 2015 over the British Isles with a particular emphasis on wind speed and direction. The band of totality for this eclipse was to the north of the British Isles with obscuration over the British Isles ranging from 83% (at Dover on the southeast English coast) to 98% (at Stornoway in the Scottish Outer Hebrides). Times of First contact, maximum eclipse and Fourth contact were 0825, 0932, and 1042 UTC respectively at Dover and 0832, 0936, 1043 UTC respectively at Stornoway.

A review of atmospheric changes from solar eclipses which includes effects on the surface temperature and circulation is presented in ref. [2]. Cooling of several °C typically occurs with the magnitude dependent on the time of day, season, extent of the eclipse (if partial) and cloud conditions. The peak cooling lags the time of maximum eclipse (if a partial eclipse) or totality (if a total eclipse) by 15–30 minutes. Relative humidity changes are typically anti-correlated with air temperature changes and increase directly as a consequence of the cooling during eclipses. For example, a 20% increase over a plant canopy in Thiruvananthapuram, India was observed during the 2010 annular eclipse (92% obscuration) associated with a 4°C drop in air temperature [3]. A reduction of specific humidity has also been reported and attributed to eclipse-induced subsidence of drier air [4].

A reduction in surface wind speed during eclipse events has commonly been reported and related to the characteristic stabilisation of the near-surface boundary layer that occurs after sunset, e.g. [2,5–7]. In contrast, ref. [8] did not observe changes in wind components that exceeded natural variability, although a reduction in the variance of the wind speed was observed. Some studies have also reported sudden increases in wind speeds or gusts at the times of First and Fourth contact of the eclipse [2,9]. These may be due to downwards turbulent mixing from a jet forming above the eclipse-induced inversion (following the mechanism responsible for the formation of the nocturnal jet) [7] or atmospheric pressure changes associated with the eclipse [10]. Changes in wind direction at have also been attributed to eclipse events although there is little consistency in type of change or attributed cause. H. H. Clayton was the first to propose (in 1901) that total eclipses modified the atmospheric circulation [11]. He observed a cold-cored anticyclonic circulation developed around the centre of the eclipse, extending outwards to about 1500 miles from the umbra. Beyond this, he observed a cyclonic circulation extending a further 1000 miles to the edge of the penumbra. Clayton attributed this cyclone to the relatively small cooling in the 'body of the atmosphere' [10]. The existence or otherwise of Clayton's 'eclipse cyclone' was the subject of debate both at the time of the eclipse (see comment [12] and Clayton's response [13]) and more recently. As described by ref. [2], some evidence consistent with the existence of of 'eclipse cyclone' has been described by several observational and modelling studies [14–16]. Other studies have also reported wind direction changes during eclipse events [5,6,17] but attributed them to synoptic evolution and/or local changes in mesoscale circulations such as sea breezes or mountain slope flows.

Determination of eclipse-induced meteorology changes requires a best estimate of how conditions would have evolved in the absence of the eclipse event. Estimating this evolution is a challenge; weather conditions change daily and evolve during the period of the eclipse event due to diurnal variations and synoptic-scale changes (e.g. the passage of fronts). In a previous

paper, [14], we diagnosed wind changes induced by the eclipse on 11 August 1999 through comparing measurements from a network of surface stations operated by the Met Office across the UK with the output of a high spatial resolution operational forecast model ignorant of the eclipse. Focusing on an inland cloud-free region (containing many measuring sites), a mean regional wind speed decrease of 0.7 $\mathrm{m\,s^{-1}}$ (1.9 knots $\equiv$ 1 $\mathrm{m\,s^{-1}}$) and backing in wind direction (anticlockwise turning in the direction the air is going towards) of 17° during the maximum eclipse hour were diagnosed. We take the same approach here to diagnose synoptic-evolution and diurnal evolution relative eclipse changes for the 20 March 2015 eclipse. Compared to the previous study of the 1999 eclipse, vastly more data are now available; we aim here to exploit this as fully as possible. Hourly measurements from two independent surface station networks (Met Office land surface stations and a network of roadside stations used for monitoring road conditions) are compared to operational output from the Met Office weather forecast model (which did not include code to represent the eclipse). Motivated by signals in the synoptic-evolution relative changes, high temporal resolution (1-minute and 20-minute data) observational timeseries from selected regions are then presented to focus on the variability in these regions.

The remainder of this paper is structured as followed. An overview of the synoptic situation is given in Section 2. The datasets used are described in section 3 beginning with observational datasets (the Met Office Integrated Data Archive System (MIDAS) land and marine surface stations dataset and Vaisala roadside dataset) and followed by the operational forecast model output. The results (Section 4) are presented in three subsections: Section 4 (a) and Section 4 (b) present the synoptic-evolution relative eclipse-induced effects on near-surface atmospheric fields deduced from the MIDAS and roadside stations respectively; Section 4 (c) presents 1-minute and 20-minute temporal resolution timeseries of the observational data. Throughout Section 4 there is a focus on the wind fields, with temperature and RH shown primarily to demonstrate consistency between the different datasets and with previous studies on eclipse effects. Section 5 summarises the findings and considers a new explanation for the observed wind direction changes and Section 6 presents some conclusions.

2. Synoptic overview

The weather situation on 20 March 2015 over the British Isles was generally cloudy with weak near-surface winds (typically less than 10 knots over England and Wales). The centre of a weak low pressure system tracked southeastwards during the morning from east of Iceland to the Scandinavian coast (Fig. 1(a) and (c)). The trailing cold front from this system cut across the British Isles and moved southwards during the morning. An upper-level cold front is marked in Fig. 1(a) and (c) to the south and east of the surface cold front at both 06 and 12 UTC on the surface analyses and a broad high pressure region existed to the south and west of the British Isles. The associated geostrophic surface winds can be inferred from the isobars marked on the surface analyses and were northwesterly over Scotland, Wales, Ireland and northern England and northeasterly over southern England and the Republic of Ireland at 06 UTC but had turned more northerly by 12 UTC. The winds were weak (inferred from the slack pressure gradients), especially to the south of the British Isles. This synoptic situation led to low-level cloud over most of the British Isles, with the exception of a clear sky band well to the south of the surface cold front (Fig. 1(b)); this zone provided good eclipse viewing conditions. At the time of the eclipse this band stretched across the Midlands from the county of Lincolnshire on the east coast and covered Wales and the county of Cornwall in southwest England. The calm meteorological conditions in the majority of the British Isles provided an opportunity to investigate possible eclipse-induced changes in surface weather data.

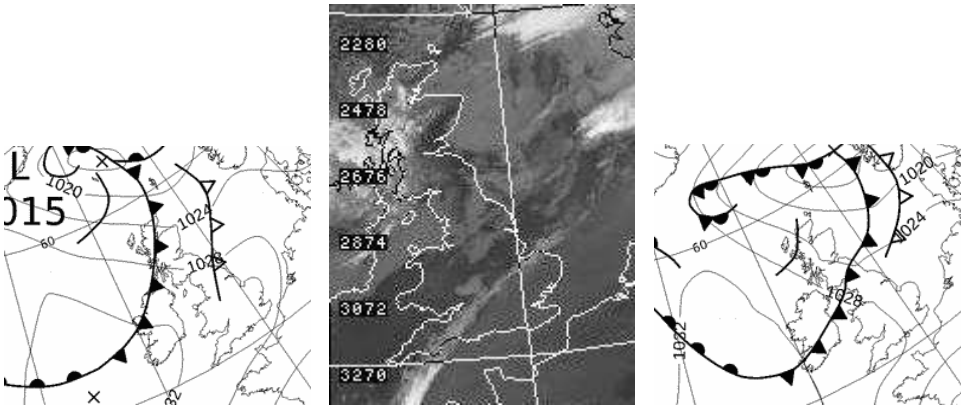

(a) (b) (c)

Figure 1. (a) Met Office surface analysis at 06 UTC, (b) Infra-red satellite image at 0922 UTC, and (c) Met Office surface analysis at 12 UTC. All for 20 March 2015. Surface analyses are © Crown copyright. Satellite image is courtesy of Dundee Satellite Receiving Station.

3. Datasets

(a) Observations

Two observational datasets are used in this study: (i) the MIDAS surface stations dataset and (ii) measurements from a network of roadside stations operated by Vaisala for monitoring road conditions. The locations of stations from each dataset (specifically those stations with temperature observations available at 12 UTC on 20 March 2015) are shown in Fig. 2. The MIDAS dataset contains land and marine surface observations from the Met Office station network across the British Isles and from other Met Office stations worldwide [18]. Hourly weather observation MIDAS data were extracted across the British Isles from the British Atmospheric Data Centre (BADC). The weather station types and message reports extracted were the same as in [14] and the same checking of quality flags was performed. Quality flags indicate the automated processing that has been performed on each measurement and whether the measurement has failed any checks. Data from 331 stations distributed across the British Isles were extracted and data were typically available (i.e. present in the station records) from about 280 stations for temperature and 220 stations for cloud and wind at the times analysed. Wind speed and direction (at 10 m height) and air temperature (at 1.25 m height) were analysed with data reported to 1 knot, 10 degrees, and 0.1°C resolution, respectively. Wind speeds and directions are 10-minute averages obtained during the 20 to 10 min prior to the reported observation hour. Wind direction observations are undefined when the wind speed is zero. It is UK practice to regard the actual observation time as 10 minutes prior to the observation hour; however, observations are assumed to apply to the observation hour in the analysis that follows. In addition to the hourly MIDAS data downloaded from BADC, one-minute temporal resolution data for wind speed and direction from the MIDAS stations were obtained directly from the Met Office. This data did not include quality flags.

The roadside observations were obtained courtesy of Vaisala, a company that develops, manufactures and markets products and services for environmental and industrial measurement. Vaisala operates on behalf of national agencies and local authorities a dense network of stations situated along the major UK highways. The stations vary in the types of measurements made and the frequency and timing of measurements (specifications for the Vaisala Road Weather Station RWS200 can be found in the product catalogue [19]) but hourly data for air temperature were provided from 868 stations across the UK. Data values were typically available from about 740, 610 and 590 stations for air temperature, wind speed and wind direction, respectively, for

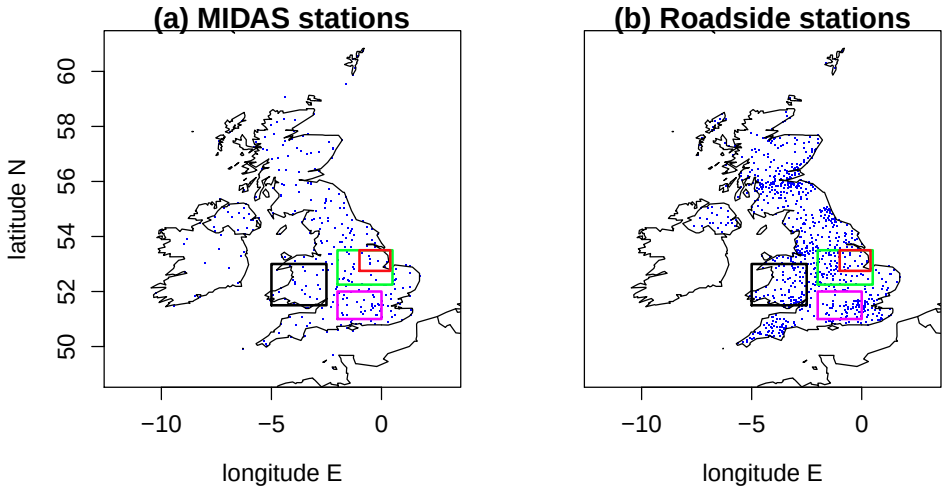

Figure 2. Locations of observational stations where temperature data are available at 12 UTC on 20 March 2015 from (a) the MIDAS dataset and (b) the Vaisala roadside dataset. Magenta, black, green and red boxes in both panels mark the 'Central southern England', 'Wales', 'Midlands1' and 'Midlands2' regions respectively, as specified in Table 1.

each time analysed. The data values do not include quality flags but come from standardised commercial products which are subject to regular calibration and maintenance to ensure validity.

Although the siting of the roadside stations is constrained by the UK road network, the majority of stations lie in relatively exposed locations away from vegetation, buildings and cuttings in order to maximise sky view factor (sky view factor is one of the main parameters affecting the behaviour of road surface temperature), reduce adverse effects on wind speed and direction, air temperature and humidity readings, and to reduce shading on the road temperature sensors particularly in low sun conditions. The aim is that the stations are sited in locations that are representative of the climatic region they represent, after allowing for power supplies and the ability to operate safely. The potential lack of representivity (for this study) arising from stations being sited according to the road network is balanced against the benefits of the very large number of stations. Almost all of the air temperature sensors are located at around 3.5 m above the ground with some of the wind instruments also located at this level. However, a large proportion of the wind instruments are located at the top of the roadside mast at about 4 m. No height corrections to the measured wind speeds are made in the data that was available. Air temperature and wind speed and direction were extracted at both hourly (whole UK) and 20-minute (selected regions) intervals for this study; although greater temporal resolution data was available for some stations, the use of 20-minute data provided the greatest number of stations operating at consistent temporal resolution. Temperature was reported to 0.1°C, wind speed to 0.1 m s^{-1} and direction to 1°.

(b) Numerical model forecast

The evolution of the meteorological variables expected in the absence of the eclipse was determined using numerical model output from an operational weather forecast produced by the Met Office following the methodology of [14]. The Met Office routinely performs weather forecasts over both the whole globe and limited-area domains initialised several times each day. Different configurations of the same Met Office model, the Unified Model, are used for both weather forecasting and climate prediction. The Unified Model is an operational finite-difference model that solves the non-hydrostatic deep-atmosphere dynamical equations with a

semi-implicit, semi-Lagrangian integration scheme [20]. The model includes full representation of physical processes through parametrization schemes. In the limited area configuration the horizontal grid is rotated in latitude/longitude to yield an approximately isotropic grid measured by Euclidean distance.

The forecast used was produced by the UK variable resolution (UKV) configuration of the model [21] with an initialisation time of 03 UTC on 20 March 2015; this forecast was chosen as the latest forecast initialised before the onset of the eclipse. The UKV model configuration has a domain that extends over the British Isles and part of Northern France. The grid spacing is 1.5 km in the inner domain, reducing to 4 km in a rim extending around the outer edges. There are 70 vertical levels on a staggered stretched grid extending up to about 70 km altitude; the lowest model levels on which temperature and horizontal wind components are held are at 5 and 2.5 m height (above the terrain) respectively. This model configuration is run operationally four times each day (initialised at 03, 09, 15 and 21 UTC using an incremental 3D-Var data assimilation scheme) out to 36 hours [21]. Most model fields are output at hourly intervals including the 2-m temperature, 2-m RH and 10-m wind components used in this study. The boundary conditions for the model come from the global model forecast which runs with coarser resolution (17-km grid spacing). The operational version of the model does not include representation of eclipses in the model code and hence the forecast produced reveals how the atmospheric state would have evolved in the absence of the eclipse. The effects of model, initial condition and boundary condition errors are assumed to be small (relative to eclipse-induced effects) given the short lead time of the forecast used.

4. Results

(a) Synoptic-evolution relative eclipse-induced anomalies deduced using MIDAS network observations

The cloud, 10-m wind and 2-m temperature conditions before (08 UTC), during (10 UTC) and after (12 UTC) the eclipse are plotted at the locations of the MIDAS stations in Fig. 3 and the left panels in Fig. 4. The eclipse maximum response in atmospheric near-surface fields generally lags the maximum eclipse time (e.g. the maximum eclipse-induced temperature anomaly lags the maximum eclipse by about 15 minutes [15]). Hence, 10 UTC is chosen to illustrate the eclipse-induced changes as this is the first available hourly data after the maximum eclipse. Data are plotted at all station points where it is available at the given times. The cloud and wind conditions (Fig. 3) can be compared to those inferred from the satellite imagery and surface analyses, respectively, shown in Fig. 1. The clear sky band across the Midlands, Wales and Cornwall at 10 UTC is evident, with stations in this zone reporting cloud cover in the range 0-2 oktas. By 12 UTC this band has moved slightly south and is now located in central southern England. The direction and relative strength of the 10-m wind vectors are generally consistent with the geostrophic winds inferred from the isobars in the surface analyses and are very weak in inland southern England (typical speed is less than 5 knots). At 08 UTC temperatures to the north of the British Isles are warmer than those to the south (typically 6-8°C in the north and 4-6°C in the south, Fig. 4(a), likely a result of less cloudy skies overnight to the south resulting in lower temperature minima there). The diurnal cycle is the dominant cause of the change in temperature during the morning (Fig. 4(a-c)) and by 12 UTC temperatures reach up to 12-14°C in central and northeast England.

Although a comparison between Figs. 4(a) and (c) indicates a lack of the expected diurnal warming between 08 and 10 UTC, the effect of the eclipse on temperature is illustrated more directly by comparison between the observed and modelled temperatures at 10 UTC. This is because comparison of the observed and forecast temperatures enables the changes in the observations resulting from the diurnal and synoptic-scale atmospheric evolution to be taken into account. The right panels in Fig. 4 show the model forecast output interpolated from

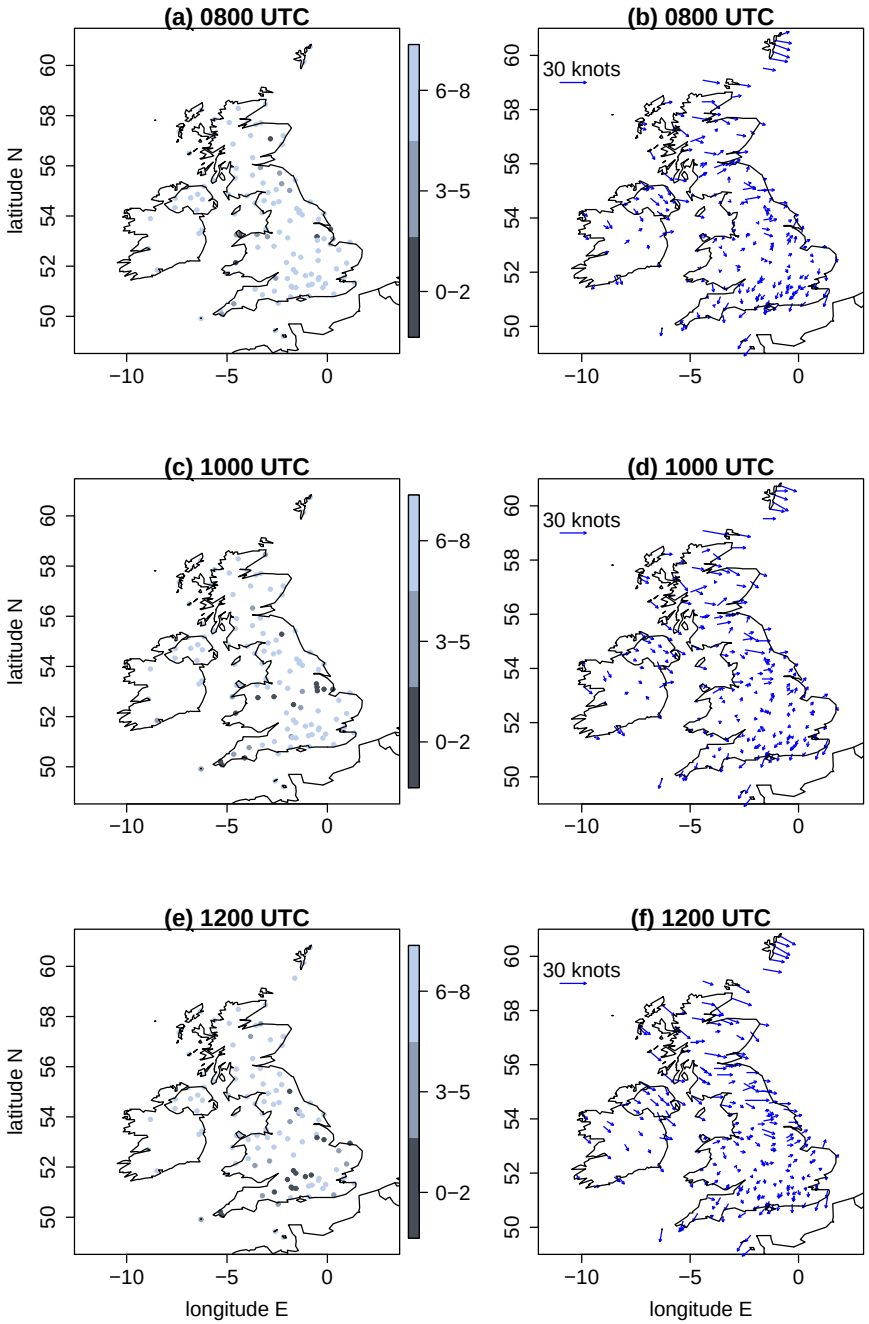

Figure 3. (left column) Total cloud cover amount at MIDAS stations (oktas) and (right column) 10-m wind vectors at MIDAS stations (with scale indicated by representative length in the upper-left of each plot) at (top row) 08, (middle row) 10 and (bottom row) 12 UTC. Note that an okta is a unit of measurement indicating the proportion of sky covered by cloud ranging from 0 (completely clear sky) to 8 (completely overcast), with a station value of 9 indicating that the sky is totally obscured.

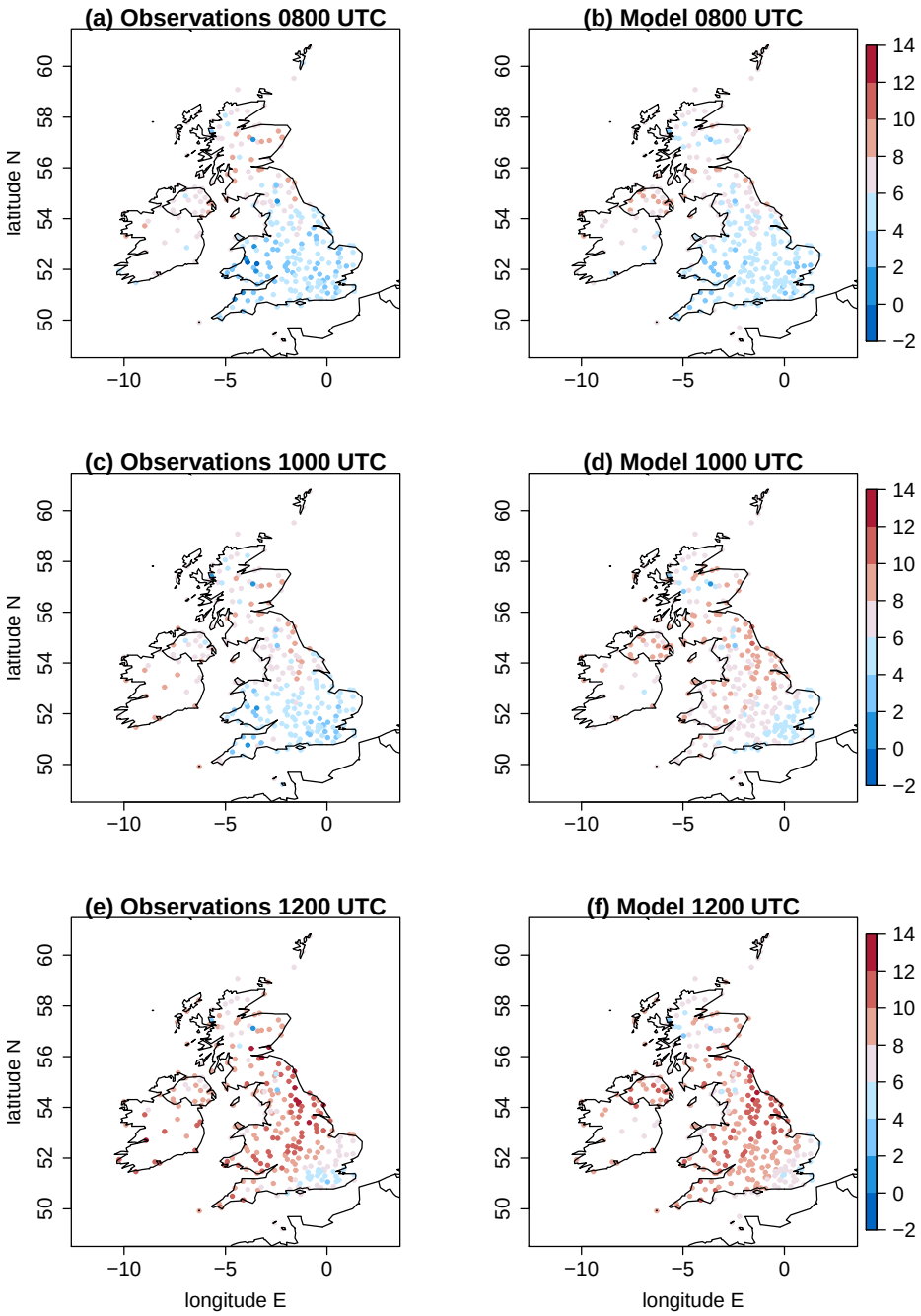

Figure 4. 2-m temperature (°C) from (left column) MIDAS stations and (right column) model temperatures interpolated to MIDAS station locations at (top row) 08, (middle row) 10, and (bottom row) 12 UTC.

the 1.5 km model grid to the locations of the MIDAS stations. At 08 UTC, prior to eclipse onset, there is a generally good agreement between the observed and forecast temperatures. At 10 UTC temperatures across the entire British Isles are cooler than forecast and this difference is particularly apparent in the clear sky band across the midlands, Wales and Cornwall

where differences reach up to approximately 4°C. By 12 UTC observed temperatures have largely recovered to match those forecast. The exception to this is in southeast England where temperatures remain lower than forecast by approximately 2°C.

Comparison of the 10 UTC observed and forecast temperatures at station points (Figs. 4(c) and (d)) provides clear evidence of eclipse-induced cooling, greatest under clear skies. However, the observed and forecast temperatures do not exactly agree even before the onset of the eclipse, and station-to-station variability in the magnitude of the observed and forecast temperature difference exists even for neighbouring stations; these differences are expected and likely result from a combination of forecast error (even at this short forecast lead time), measurement error, and the interpolation of the model data to the station points (which does not take altitude changes into account). Figure 5(a) illustrates this difference (observed minus forecast temperature) at 09 UTC. To allow for these differences existing before eclipse onset, Figs. 5(c) and (e) show the change in the temperature difference (observed minus forecast temperature) from 09–10 UTC and 10–11 UTC respectively. These changes are termed 'synoptic-evolution relative' changes hereafter and the magnitude of these changes should be considered relative to the difference in temperature between observed and modelled temperature prior to eclipse onset. To smooth the station to station variability, the panels of Fig. 5 show difference fields at station points averaged over boxes of 1°longitude and 0.5°latitude (roughly square in Euclidean distance at this latitude). The time from when the synoptic-evolution relative temperature changes are determined (09 UTC) is after the onset time of the eclipse over the British Isles. This time was chosen to enable the changes to be determined over a 1-hour period focused on the time period of the likely greatest eclipse-induced changes. Considering this 1-hour period will reduce uncertainty associated with the differences between the observations and forecast by providing an estimate of these differences at a time as close as possible to the time when the maximum eclipse-induced changes are expected (within the constraint of the hourly-forecast data availability). For example, the maximum temperature anomalies are expected to have occurred at about 0945 (about 15 minutes after the maximum eclipse at about 0930).

At 09 UTC observation minus forecast differences in temperature are typically within $\pm 1^{\circ}$C, with generally negative values to the south and positive values to the north of the British Isles (Fig. 5(a)). The north-south difference could suggest that the eclipse may have already induced a weak cooling in the clearer skies to the south (e.g. the obscuration was already about 45% at Reading in Berkshire at 09 UTC), but a similar difference already exists at 08 UTC (compare Figs. 4(a) and (b)). The synoptic-evolution relative temperature change from 09–10 UTC is negative across the entire UK (isolated positive changes exist in the Republic of Ireland) implying eclipse-induced cooling occurred; typical magnitudes are 1-3°C (Fig. 5(b)). Many of the averaging boxes with the larger temperature changes occur in the clear sky band. Comparing the temperature change from 10–11 UTC with that from 09–10 UTC the sign is generally reversed, implying a warming in the observations relative to the forecast over this period and so a recovery from the eclipse-induced cooling. This is consistent with the improved agreement between observed and forecast temperatures an hour later at 12 UTC (compare Fig. 4(e) and (f)). The exception to this recovery is in southeast England which is associated with further (though weak) cooling from 10–11 UTC.

Changes in RH have previously been attributed to eclipse events (see Section 1) and the right hand panels of Fig. 5 illustrate the synoptic-evolution relative RH changes in the same format as the temperature changes shown in the left hand panels. At 09 UTC the observations and forecast RH values generally agree within $\pm 10\%$ with some larger differences found over Wales, southwest England and Scotland (where local high and variable orography and coastal effects might be expected to lead to larger differences as the interpolation of the forecast data to the station points will be less representative). The synoptic-evolution relative RH changes from 09–10 UTC are generally positive, implying an eclipse-induced RH increase of the air relative to the synoptic evolution, and reach 5–20% in the clear sky band. Changes from 10–11 UTC are generally negative across England and Wales (with the exception of southeast England) implying

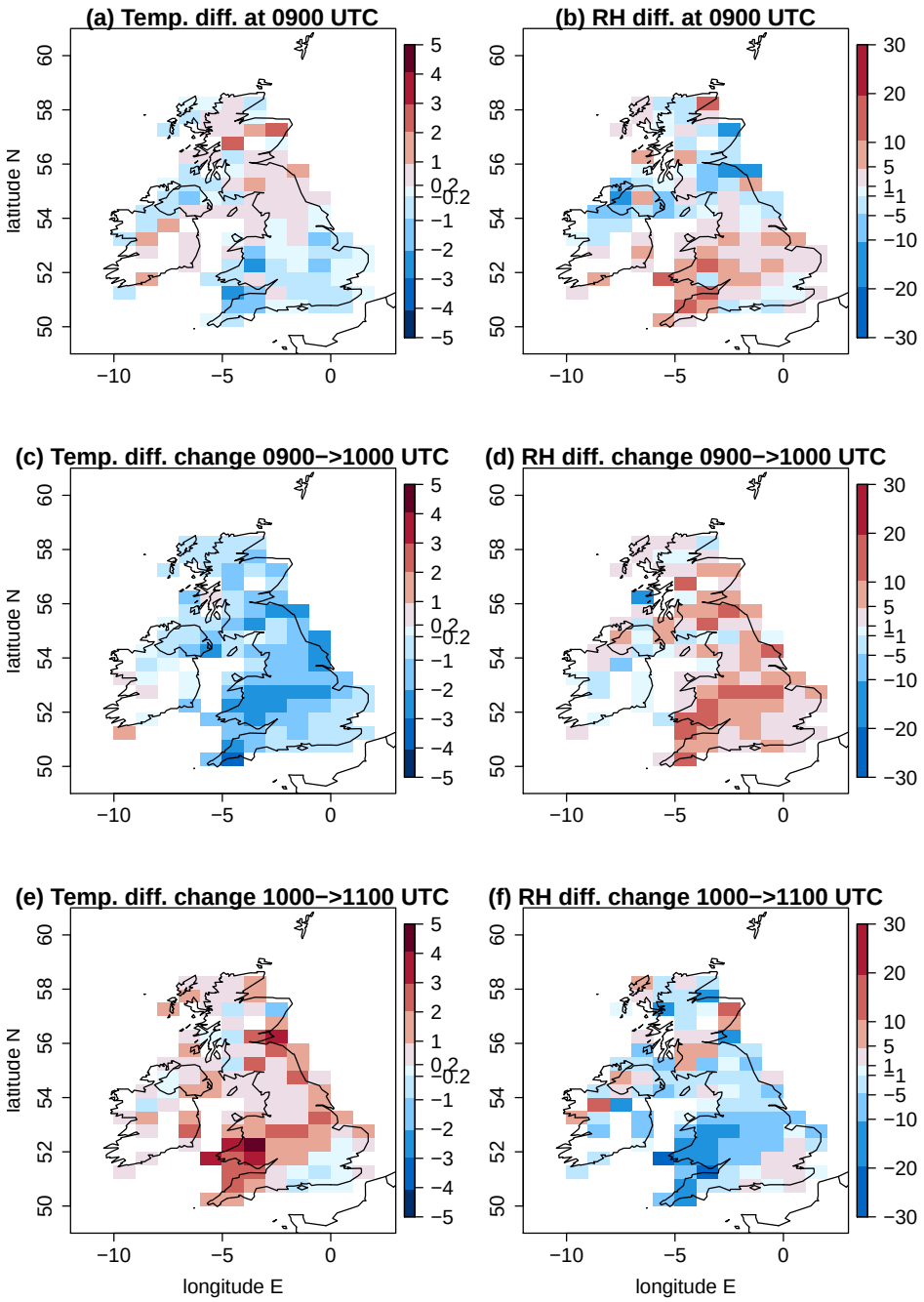

Figure 5. (top row) MIDAS observations minus model difference for (a) 2-m temperature (°C) and (b) 2-m RH (%) at 0900 UTC. (middle row) Change in (observation - model) difference between 0900 and 1000 UTC for (c) temperature and (d) RH. (bottom row) As for middle row but for change in difference between 1000 and 1100 UTC. A positive value for temperature difference or change in difference indicates either warmer observed relative to modelled temperature (top row) or a warming with time of the observed relative to the modelled temperature (middle and bottom rows). A positive value for RH difference or change in difference indicates either increased observed relative to modelled RH (top row) or an increase with time of the observed relative to the modelled RH (middle and bottom row). Station values are averaged over 1° longitude by 0.5° latitude regions. Small magnitude values are shaded light grey (-0.2 to 0.2°C; -1 to 1%).

a recovery (RH decrease) of the air towards the values that would have occurred in the absence of the eclipse. The RH changes are anticorrelated with the temperature changes implying that cooling associated with the eclipse leads to the RH increase and that this effect dominates over that due to any decrease in specific humidity. The typical magnitudes of the RH increase are also consistent with those expected from cooling at constant specific humidity: for example, a cooling of 4°C at 10°C for constant specific humidity should lead to an RH increase of about 20%.

Eclipse-induced effects on temperature and RH are well understood and documented. In contrast, the effects on wind speed and direction are more controversial (see Section 1). Figure 6 shows the synoptic-evolution relative changes in wind speed and direction in the same format as in Fig. 5. At 09 UTC observed wind speeds and directions are generally within ± 2 knots and $\pm 40^{\circ}$ of the forecast values over southern England, but larger differences exist elsewhere, especially over Scotland for wind speed and Wales for wind direction. As with the RH field, larger differences over high and variable orography are not surprising; note also that the stations are less densely located over Scotland and Wales than in England (see Fig. 3(b), (d), and (f)) reducing the smoothing effect of the box averaging. Focusing on England, a generally negative synoptic-evolution relative change in wind speed occurs from 09–10 UTC of up to 4 knots followed by further changes of typically ± 2 knots from 10–11 UTC with increases slightly dominating over decreases. These changes imply a reasonably consistent eclipse-induced weakening of the winds followed by some signs of a recovery. The changes are less consistent across the British Isles than the equivalent changes in temperature and RH. This can partly be attributed to the very weak winds over England at this time (see Fig. 3(b), (d), and (f) and note that cup anemometers also have a starting wind speed, i.e. a minimum wind speed that can be recorded, which is typically $\sim 1-4$ knots [22]). Synoptic-evolution relative changes in direction are also not very consistent across the British Isles (Fig. 6(d), (f)). However there is a generally positive synoptic-evolution relative wind direction change across England from 09–10 UTC followed by a generally negative change from 10–11 UTC. In the calculation, a positive change means that the angle anticlockwise relative to East that the wind vector points towards in the observations has increased relative to that angle in the forecast and so a backing of the wind direction; a negative change implies the observed wind direction has veered relative to the forecast. Hence, we conclude that the synoptic-evolution relative wind evolution reveals a reasonably coherent weakening in the (already weak) wind speeds and the suggestion of a backing of wind direction over England during the eclipse.

The lack of strongly robust eclipse-induced wind response motivates a further analysis using the independent roadside station network, which has an enhanced density of measurement sites.

(b) Synoptic-evolution relative eclipse-induced anomalies deduced using Vaisala roadside network observations

The greater density of the roadside network stations compared to the MIDAS stations used and general consistency of the temperature and winds measured there with those from the MIDAS station network (and model forecast prior to eclipse onset) can be seen by comparison of Fig. 7 with Fig. 3 (right panels) and Fig. 4. (Note that roadside observations were not available for the Republic of Ireland.) The roadside station temperatures are very consistent with the MIDAS station observations and forecast generally the same temperatures (in the same regions) within the 2°C discretisation used for plotting. The warmest roadside station temperatures slightly exceed those from the MIDAS stations which accounts for the warmest colour band covering 4°C in Fig. 7 (left column) instead of 2°C as in Fig. 4. The wind speeds measured by the roadside stations are generally weaker than those measured by the MIDAS stations. This is likely to be attributable to the lack of numerical adjustment of the height of wind measurements from the measurement height to 10 m (as is performed where required for the MIDAS observations). The wind directions across the UK from the roadside and MIDAS observations are regionally consistent.

Figure 8 shows the synoptic-evolution relative changes in wind speed and direction for the roadside observations; this is derived in the same way as for the MIDAS observations shown in

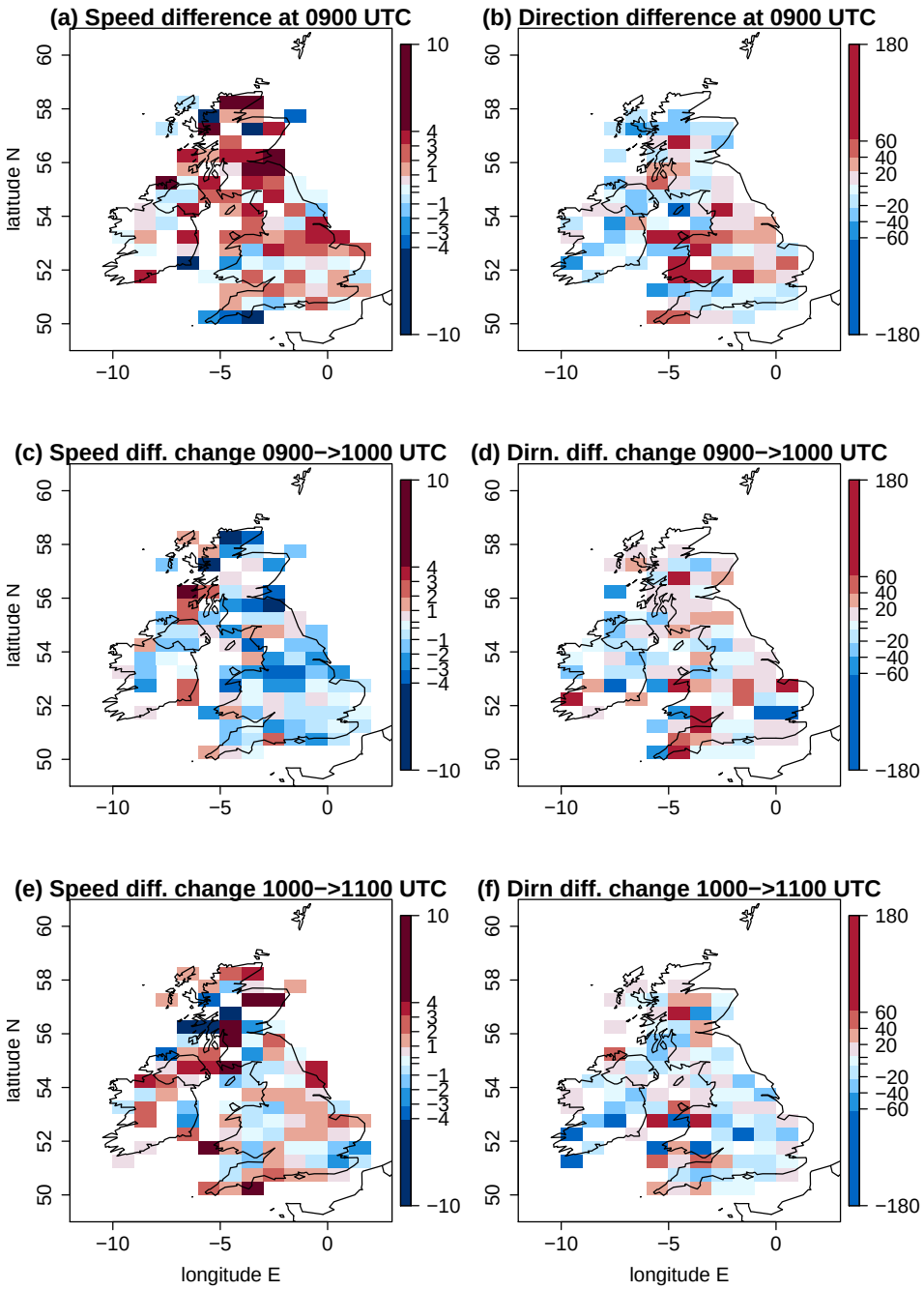

Figure 6. (top row) MIDAS observations minus model (interpolated to station locations) difference for (a) 10-m speed (knots) and (b) 10-m direction (°) at 0900 UTC. (middle row) Change in (observation - model) difference between 0900 and 1000 UTC for (c) speed and (d) direction. (bottom row) As for middle row but for change in difference between 1000 and 1100 UTC. A positive value for speed difference or change in difference indicates either stronger observed relative to modelled wind (top row) or a strengthening with time of the observed relative to the modelled wind (middle and bottom rows). A positive value for direction difference or change in difference indicates either a backed observed relative to modelled wind (top row) or a backing with time of the observed relative to the modelled wind (middle and bottom rows). Station values are averaged over 1° longitude by 0.5° latitude regions. Small magnitude values are shaded light grey (-0.2 to 0.2 knots; -4 to 4°). Note that in panel (a) there is one data value of -14 knots; this is shaded in the colour indicted as the -10 to -4 knot range.

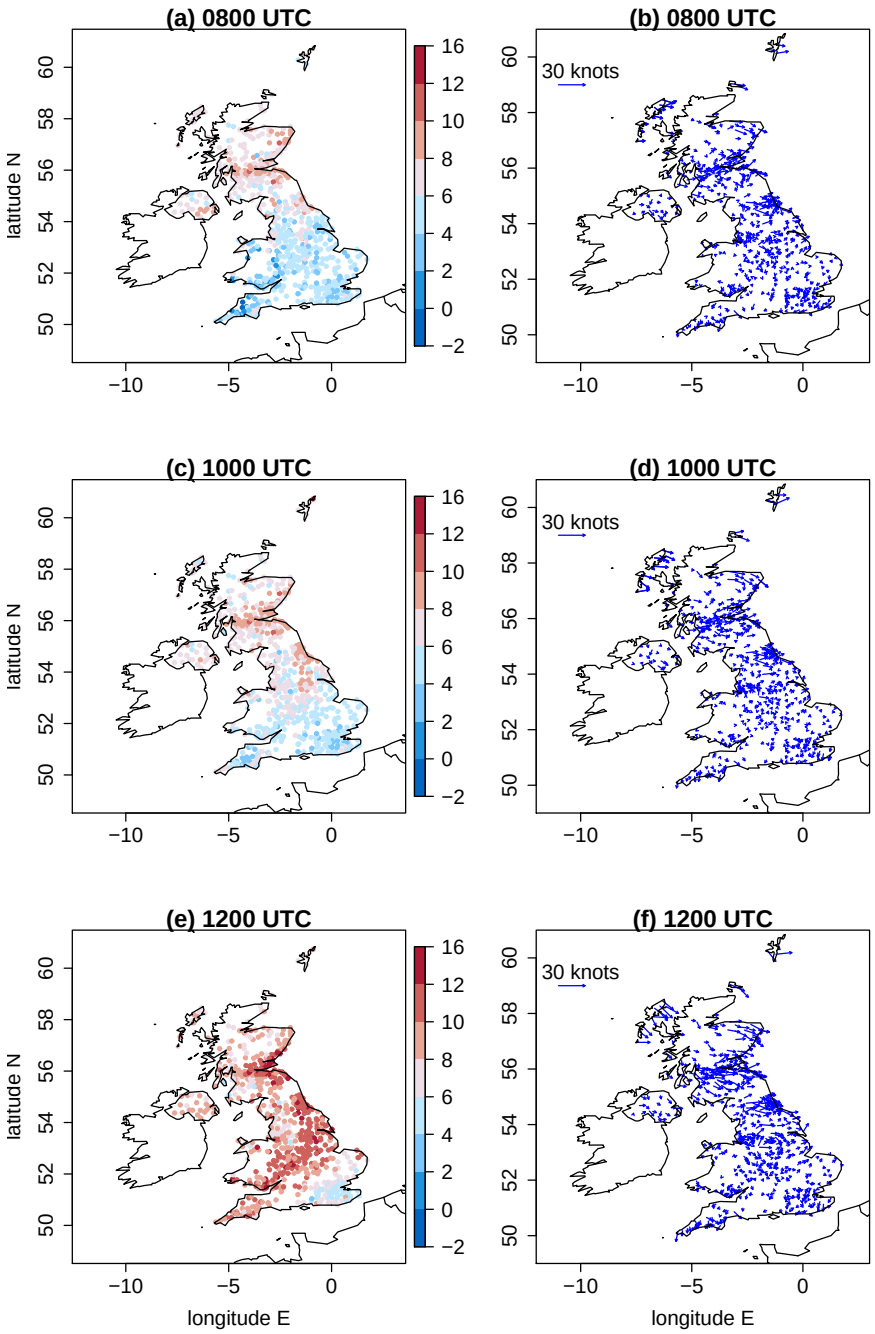

Figure 7. (left column) temperature at roadside stations and (right column) wind vectors at roadside stations at (top row) 8, (middle row) 10 and (bottom row) 12 UTC.

Fig. 6. Overall the fields plotted appear more spatially coherent for the roadside observations than for MIDAS observations, especially over England and Wales; this is likely a consequence of the greater density of stations for the roadside observations. At 09 UTC the observed wind speeds can be seen to be generally weaker than the forecast winds by 1–2 knots over Wales and inland

England areas though by more over Scotland and along the southern UK coast where winds were stronger (Fig. 8(a)). This may partly be attributable to the eclipse since 09 UTC is after eclipse onset (although the observed MIDAS wind speeds were generally stronger than the forecast ones at 09 UTC (Fig. 6(a)); other likely reasons for this are discussed above based on comparison of the roadside and MIDAS wind vectors. Observed roadside wind directions are generally within $\pm 20^{\circ}$ of those forecast (Fig. 8(b)) with a slight preference for the observed winds to be backed relative to those forecast, as also found with the MIDAS observations (Fig. 6(b)). The synoptic-evolution relative changes in roadside wind speed and direction from 09–10 UTC and from 10–11 UTC are consistent in sign with those found for the MIDAS observations, especially over England, and the greater spatial coherence of the patterns lends confidence that they are robust.

These robust synoptic-evolution relative changes now motivate the closer examination of high temporal resolution (1-minute and 20-minute data) observations from selected stations.

(c) Regional eclipse-induced surface meteorological change deduced from high temporal resolution observations

The advantage of analysing 1-minute and 20-minute temporal resolution station data is that eclipse-induced changes occurring on timescales of less than an hour can be resolved. The disadvantages are that synoptic-evolution relative changes cannot be easily determined for comparison (the operational model output is only available on the hour for fields analysed here) and the one-minute MIDAS wind data are very noisy compared to the hourly MIDAS wind data (which is provided as an average over a 10-minute period). Figures 9 to 12 show wind speed and direction data at one-minute (MIDAS observations) and 20-minute (roadside observations) intervals for four selected regions; these regions are marked on Fig. 2 and the specifications are given in Table 1. The selection of these regions was motivated by the robust eclipse-induced changes in wind speed and direction (relative to the synoptic evolution) found over England in Sections 4.(a) and (b) and the preferential occurrence of large eclipse-induced changes in temperature and RH in the clear sky band across the midlands, Wales and Cornwall. The Wales and Midlands1 regions were selected as covering the cloud free regions over central England at 10 UTC. Midlands2 is a subregion of Midlands1, chosen to focus on the clearest region and such that there is consistency in the wind speed station data for the stations chosen (i.e. the evolutions of wind speed and direction follow tight plumes). The central southern England region was selected as a cloudy inland region just south of the cloud-free band with lots of stations. Figures 9 to 13 show the data from individual stations (thin grey lines) and mean values (bold red lines) with error bars. UKV model forecast output interpolated to the station locations is also shown in the panels showing the one-minute MIDAS data (Figs. 9 and 10) and the temperature and RH values for the 20-minute roadside data (Fig. 13). In Figs. 9 and 13 the model output data are shown in box and whisker format; in Fig. 10 the orange diamonds mark the model values at the stations and black diamonds mark the mean of the station values. Stations within the regions that recorded zero wind speed at any time within the limits plotted were excluded from the analysis so as not to bias the mean values of wind speed and wind direction (direction is undefined when speed is zero). This constraint removed several stations from analysis, particularly in the Wales region where the winds were weakest.

Table 1. Specification of regions. The location of the regions is shown in Fig. 2.

Region	Latitude limits (°N)	Longitude limits (°E)	Comment
Central southern England	51, 52	-2, 0	Cloudy, inland
Wales	51.5, 53	-5, -2.5	Clear band
Midlands1	52.25, 53.5	-2, 0.5	Clear band
Midlands2	52.75, 53.5	-1, 0.4	Clear band; subset of Midlands1

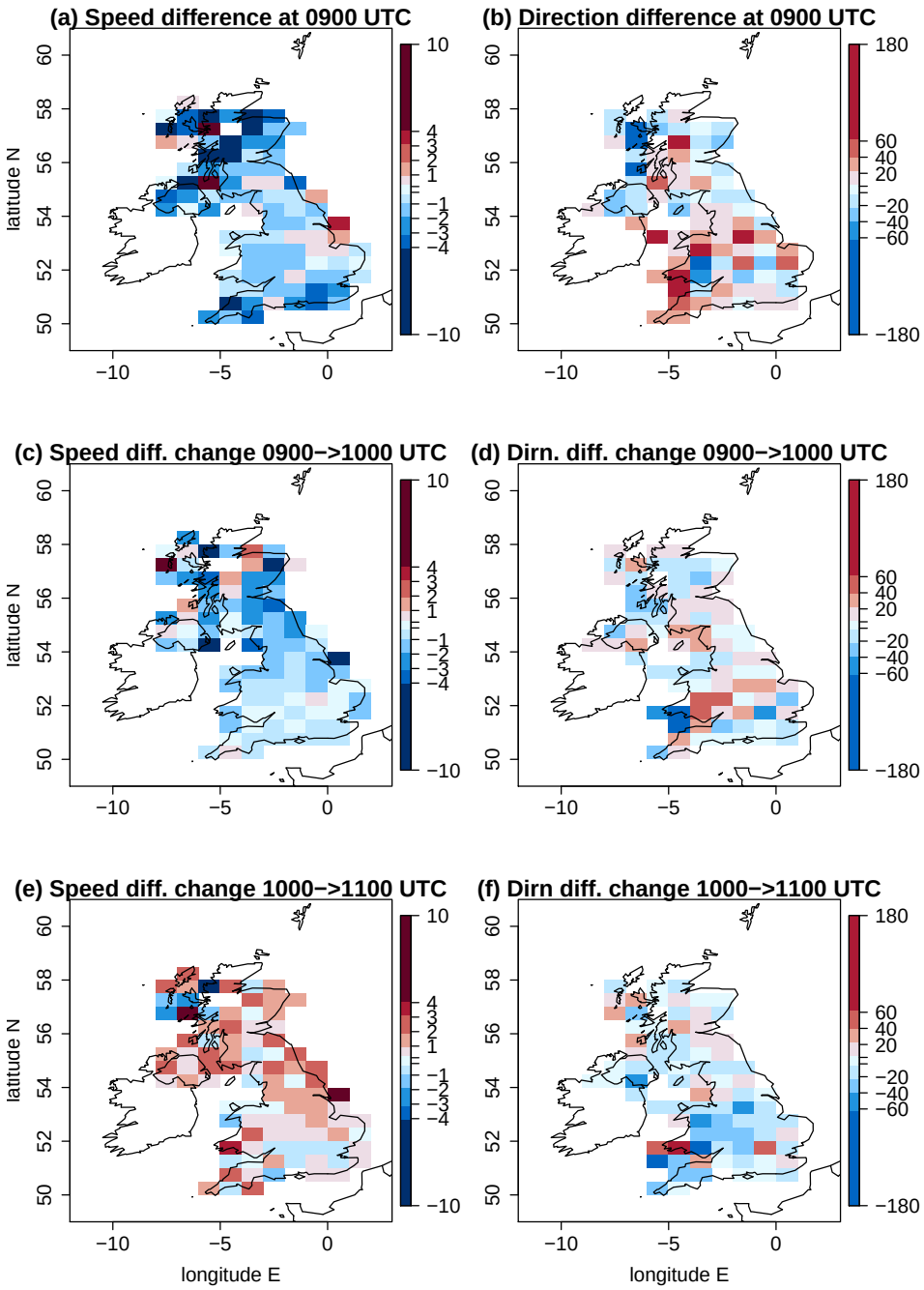

Figure 8. As for Fig. 6 but for comparison of the roadside observations with the model. All data values are within ranges indicated on the colour bars.

Beginning with the one-minute MIDAS observations, Fig. 9 shows that wind speeds evolved due to synoptic evolution and the diurnal cycle during the time period shown (gradually decreasing on average over the central southern England region for example). However, within this evolution, over a several hour timescale, a more rapid evolution can be discerned around the

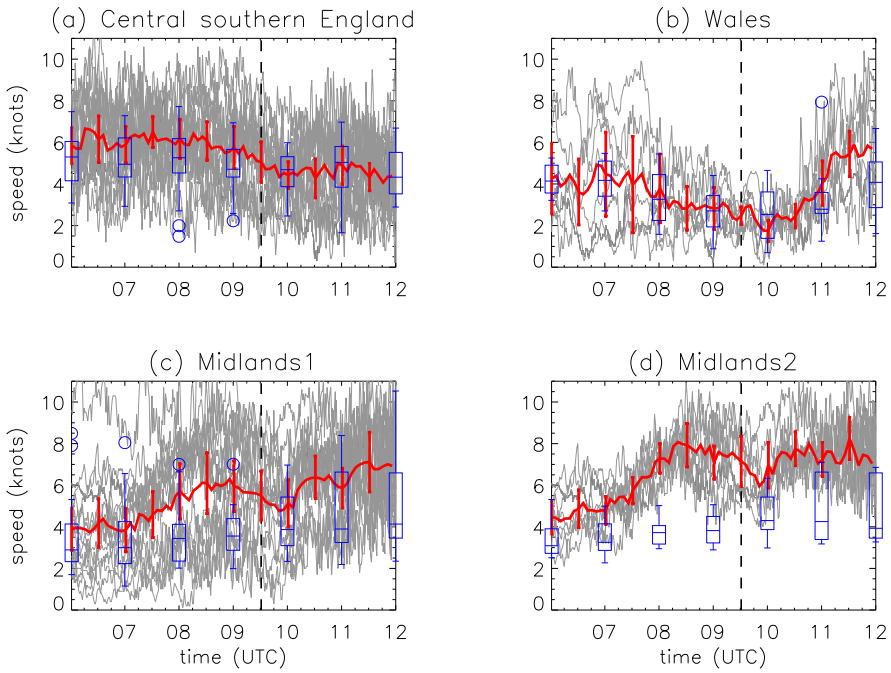

Figure 9. One-minute temporal resolution MIDAS 10-m wind speed data (knots) as a function of time for sets of stations in four regions: (a) central southern England; (b) Wales, (c) Midlands1, and (d) Midlands2. Stations are selected within the latitude and longitude limits at which one-minute wind speed data are available at all times and the speed is non-zero at all times. Vertical dashed line marks the approximate time of the maximum partial eclipse (0930 UTC). Thick red line shows the mean value with error bars given by $\pm 1.96\times$ standard deviation (yielding the 95% confidence interval). Model forecast values interpolated to station locations are overplotted in blue in box and whiskers format. The box encloses the interquartile range with the horizontal line marking the median value. The whiskers extend out to the maximum or minimum value of the data, or to 1.5 times either the 1st or 3rd quartile if there is data beyond this range. Outliers are identified with circles. Number of stations plotted is (a) 17, (b) 7, (c) 16 and (d) 8. The upper bound of speeds plotted is limited for clarity so data from individual stations occasionally exceeds this.

time of the eclipse (the approximate time of the maximum partial eclipse, 0930 UTC, is marked by the bold dashed line). A reduction in wind speed from about 09–10 UTC is clearly evident in the central southern England and Midlands regions (in the central southern England region this the post-eclipse increase is somewhat obscured by the general reduction in wind speed during the period shown). Over Wales, a reduction in the range of wind speed during the eclipse is more apparent than a reduction in the mean wind speed. The reduction in wind speed of about 2 knots is followed by a rapid recovery in the Midlands1 and Midlands2 regions over about 15 minutes. In contrast, the wind speeds forecast by the UKV model do not undergo a rapid reduction around the time of the eclipse. The wind speeds are under-predicted by the forecast in the central southern England, Midlands1 and Midlands2 regions prior to the eclipse and so are a better match to those observed after the eclipse. In the Wales region, the mean forecast wind speed is a good match to that observed throughout the period plotted; however, a reduction in the spread across stations is not observed in the forecast wind speeds, unlike in the observations. While the effect of other forcings on the wind speed cannot be ruled out, the change observed around the time of the eclipse is attributed here to the eclipse due to its rapidity, the lack of similar wind speed changes in the model forecast winds, and the consistency of the wind speed changes with those observed in other eclipse events.

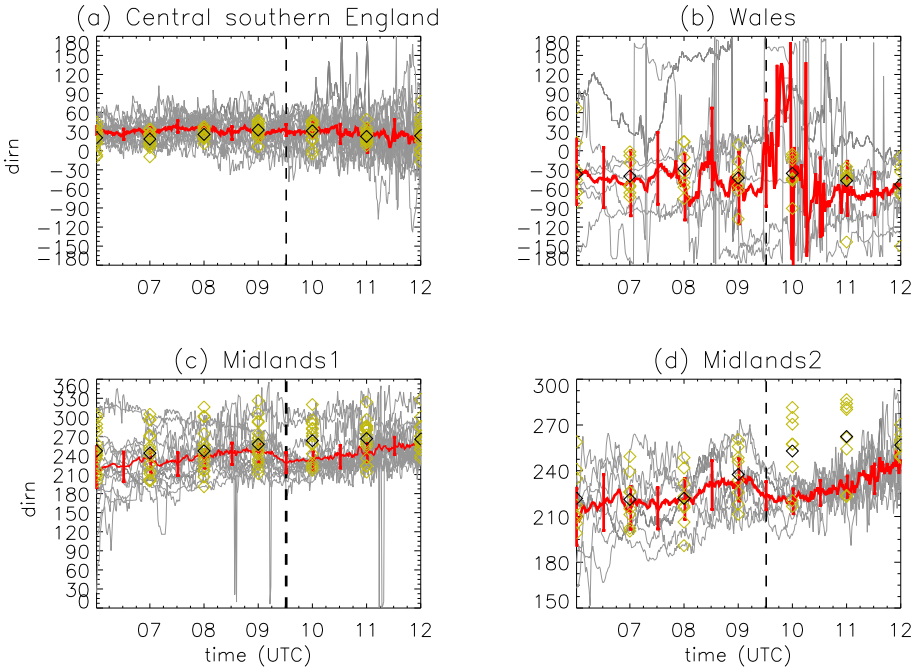

Figure 10. As Fig. 9 but for wind direction. Wind directions are described conventionally, as the angle clockwise from North that the wind is coming from (e.g. an angle on 90° is an easterly wind). Stations are selected within the latitude and longitude limits at which one-minute wind speed data and direction data are available at all times and the speed is non-zero at all times. Model forecast values interpolated to station locations are overplotted in orange diamonds (rather than as box and whiskers as in Fig. 9); black diamond denotes mean values. Number of stations plotted is the same as in Fig. 9. Note y-axis varies between panels.

In Fig. 10 a backing from about 0900–0930 UTC by about 20°, followed by a slow veering, in the wind direction during the eclipse is clearly evident in the Midlands1 and Midlands2 regions. There is no obvious wind direction change associated with the eclipse over the cloudy central southern England region. Over Wales the wind directions are very variable, as expected given the hills and mountains in this region which can dominate local wind flows; it is not possible to discern an eclipse-induced wind direction change in this region. The forecast wind directions are a good match to those observed over the central southern England and Wales regions (although the observed range of directions is enhanced after the eclipse relative to the model forecast). In the Midlands1 and Midlands2 regions the forecast and observed wind directions are a good match until 09 UTC after when the forecast winds continue to veer whereas the observed winds back leading to a difference of about 30° at 10 UTC. The timescale of the wind speed and direction changes attributable to the eclipse is about 1 hour which provides rationale for the calculations of synoptic-evolution relative changes over one-hour periods presented in Figs. 5, 6 and 8.

The 20-minute roadside observations have similar temporal evolutions to the one-minute MIDAS observations. The wind speeds are generally weaker in the roadside observations (e.g. compare Fig. 11(a) with 9(a)) which is consistent with the systematic bias seen across the entire UK and discussed in section 4. (b). A reduction in mean wind speed of about 2 knots from about 09–10 UTC is evident in the Wales, Midlands 1 and Midlands2 regions but not discernable in the central southern England region (Fig. 11(a)). The roadside observation wind direction timeseries for the Midlands1 and Midlands2 regions show the same pattern of backing followed by veering during the eclipse period as the equivalent MIDAS observation plots (compare Figs. 12(c,d) and 10(c,d)) although the wind directions are more widely spread within the each region. In the central

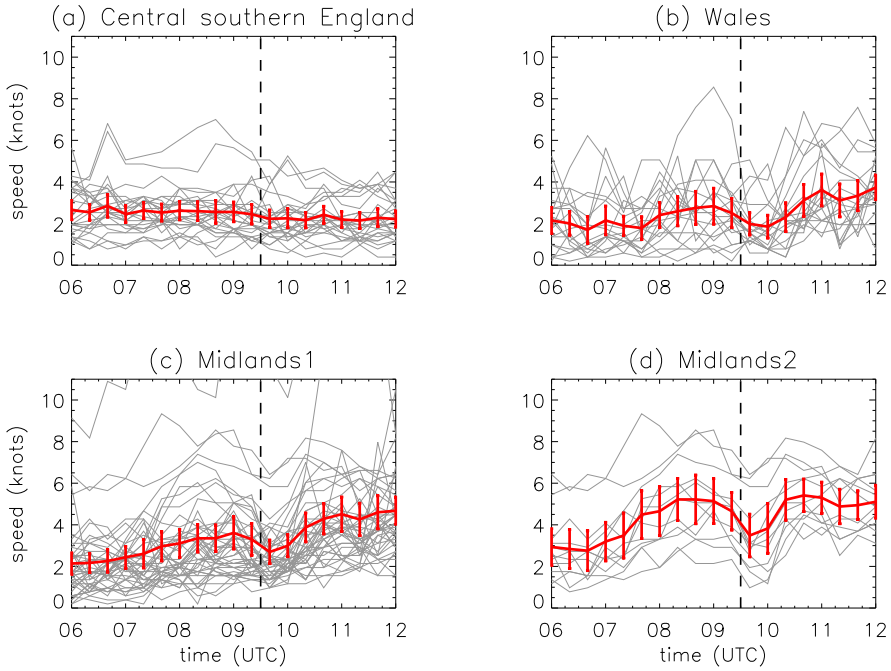

Figure 11. As Fig. 9 but for 20-minute temporal resolution roadside wind speed data. Number of stations plotted is (a) 26, (b) 19, (c) 44 and (d) 12.

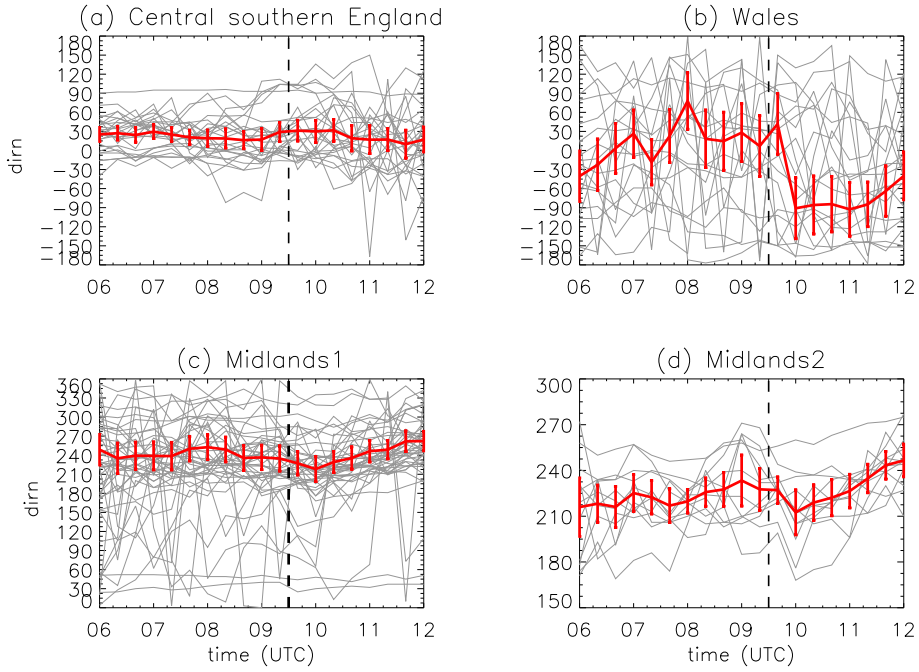

Figure 12. As Fig. 11 but for wind direction. Number of stations plotted is the same as in Fig. 11.

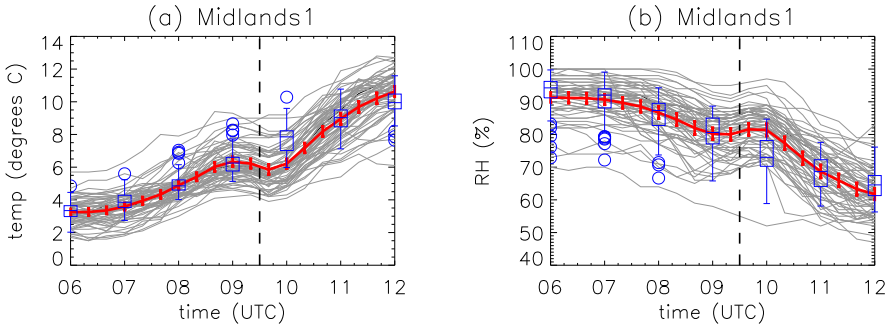

Figure 13. 20-minute temporal resolution roadside observations as a function of time for (a) temperature and (b) RH in the Midlands1 region only. Stations are selected within the latitude and longitude limits at which 20-minute (a) temperature and (b) RH data are available at all times. Vertical dashed line marks the approximate time of the maximum partial eclipse (0930 UTC). Thick red line shows the mean value with error bars given by $\pm 1.96\times$ standard deviation (yielding the 95% confidence interval). Model forecast values interpolated to station locations are overplotted in blue in box and whiskers format (as in Fig. 9). Number of stations plotted is 62 (for both fields).

southern England region (Fig. 12(a)) the mean direction veers during the eclipse period relative to the direction before and after the eclipse although this does not seem to be directly attributable to the eclipse as the veering takes place transiently during the 20 minutes after 09 UTC, and is not sustained throughout the eclipse. In the Wales region (Fig. 12(b)) the mean wind backs sharply at 0940 UTC. The large variability in the wind directions in this region together with the sharpness of the backing suggest that this change also cannot be attributed to the eclipse.

Confidence in the wind speed reduction and backing attributed to the eclipse can be qualitatively assessed from the size of the changes during the eclipse compared to the size of the error bars plotted in Figs. 9 to 12 (the error bars indicate the 95% confidence interval in the mean). The error bars are generally statistically smaller for the roadside observations than for the MIDAS observations due to the larger number of available stations. The highest confidence in the eclipse-induced changes is found by considering the Midlands1 region, the larger of the two Midlands regions located in clear skies, and the roadside data. The size of the eclipse-induced anomalies can only be approximated from the plots since the effects of the synoptic and diurnal evolutions cannot be precisely quantified. The estimated wind speed reduction of about 2 knots exceeds the confidence interval of 1.3 knots calculated at 0930 (Fig. 9(c)). However, the estimated backing of about 20° is about half the confidence interval of 38° and hence cannot be considered robust. Confidence in the changes in these wind fields can be contrasted with that in temperature and RH. Figure 13 shows the temporal evolution of temperature and RH from the roadside observations in the Midlands1 region. Both fields clearly fail to completely recover from the eclipse-induced changes leading to a lag in the morning warming and RH reduction of the near-surface air. Despite this complication, the eclipse-induced changes of perhaps 1°C and 10% clearly exceed the confidence intervals (calculated as 0.6°C and 3.6% at 0930).

5. Discussion

An analysis has been presented of the near-surface atmospheric anomalies over the British Isles attributable to the partial solar eclipse of 20 March 2015. Previous research has demonstrated consistent cooling and associated RH increase associated with eclipse events. However, the wind field response has been more unclear with some researchers identifying a response and others not. To account for the synoptic-scale evolution during the eclipse, eclipse-induced anomalies have been determined through comparison of meteorological observations against the output

of a state-of-the-art high resolution operational weather forecast over the UK; the solar eclipse was not represented in the model code and so the forecast provides a 'best guess' of the forecast evolution that would have occurred in the absence of the eclipse. Two types of meteorological measurements were analysed: (i) measurements from the MIDAS Land Surface Stations (both hourly observations over the British Isles and one-minute observations from selected stations) and (ii) measurements from a roadside measurement network operated by Vaisala to monitor road conditions. The roadside network is extensive over the UK with 868 stations used compared to the 331 MIDAS stations from which hourly weather observations were obtained. Whereas the MIDAS dataset is routinely used for British Isles meteorological analysis, we believe this is the first meteorological analysis using the unique roadside network dataset.

Weather conditions for observing eclipse-induced surface weather changes were poor over most of the British Isles with widespread cloud and relatively weak winds. However, a band of clear skies extended across middle England, Wales and into northern Cornwall. Hence, in addition to the British Isles-wide analysis presented here, 1-minute and 20-minute observations have been presented from regions within this clear sky band and from a region with contrasting weather conditions: cloudy central southern England. MIDAS wind and cloud observations over the British Isles are consistent with the Met Office surface analyses (in terms of direction and relative strength as inferred from the isobars) and satellite imagery. MIDAS temperature observations show show the expected diurnal warming during the morning and comparison with the model output illustrates the cooling attributable to the eclipse (reaching up to 4°C at station points in the cloud-free regions).

Synoptic-evolution relative eclipse-induced gridded (1° longitude by 0.5° latitude grid box averages) temperature anomalies and RH anomalies (inferred from comparing the changes in the MIDAS observations with those from an operational model forecast ignorant of the eclipse) reach up to 3°C and 20%, respectively, in the cloud-free band. Synoptic-evolution relative eclipse-induced gridded wind speed and direction changes are less homogeneous across the UK than for temperature and RH but, focusing on the clear sky band, there is reasonably consistent weakening (by up to 2 knots in the already weak winds) and backing in the wind direction (by 20-40°) during the eclipse followed by a somewhat consistent strengthening and veering after the eclipse.

The temperature and wind evolution during the eclipse from the roadside observations are consistent with those in the MIDAS observations although the winds are generally weaker. This difference is likely attributable to a lack of numerical adjustment of the height of wind measurements from the measurement height to 10 m (as is performed where required for the MIDAS observations); sheltering of the roadside stations may also contribute. The larger number of roadside stations is highly advantageous as it yields smoother gridded wind speed and direction distributions over the UK compared to the MIDAS dataset. A consistent weakening and backing followed by strengthening and veering compared to the model output is found fairly consistently across the clear sky regions in middle England and Cornwall.

High temporal resolution (1-minute and 20-minute data) observations for stations within three clear sky regions and one cloudy region illustrate the timescales during which the eclipse-induced wind changes occur. Wind speeds slacken from shortly before 09 UTC to nearly 10 UTC by up to about 2 knots in all regions at the MIDAS stations and three of the four regions at the roadside stations (the exception being the cloudy central southern England region). Backing of about 20° occurs over the same timescale although this is only evident in the clear sky Midlands regions (at both station types); no clear directional changes are observed in the cloudy central southern England region and the directional changes are highly variable in the Wales region (hypothesised to arise due to local slope-induced flows in this orographic region). The sign and magnitude of these regional changes are consistent with those determined from MIDAS observations from the 11 August 1999 eclipse over the UK (0.7 m s^{-1} and 17°) [14]; this eclipse was at its maximum over the UK (total over southwest UK) at about 1015 UTC, so at a similar time of day to the 20 March 2015 event. This consistent wind response during two different eclipse events and determined

using two independent observational networks provides confidence that wind direction changes occur robustly during eclipse events over inland regions with low orography.

The backing of the wind direction observed during the eclipse is reminiscent of the changes in wind direction which can also occur at sunset leading, in some circumstances, to a jet — the nocturnal jet — of relatively enhanced wind speeds above the surface [23,24]. The situation leading to a nocturnal jet was originally studied by [25]; [26] used a layer model to consider the effect of surface friction on the jet and showed that the jet maintained its increased speed through decoupling of the jet from the surface. This decoupling minimises the surface drag on the flow, a further consequence of which is a change in wind direction. Wind direction changes can also occur without the full decoupling of the flow associated with the nocturnal jet, if the relative effects of surface drag, the pressure gradient force and Coriolis acceleration change. A change in the boundary layer depth can lead to such wind direction changes. During a typical convective cloudy day, a convective boundary layer steadily develops which then transitions to a shallow stable layer after sunset e.g. [27]. The circumstances of a substantial eclipse are similar, but the changes occur more rapidly. Wind profiles of the whole boundary layer were obtained using a Ultra High Frequency (UHF) band Doppler Radar during the 11 August 1999 eclipse by [28], who reported appreciably lessened reflection from the boundary layer top, associated with a suppression of turbulence and boundary layer reduction. A decline in the boundary layer height was also directly observed during the 29 March 2006 solar eclipse in Greece by [29] who showed, using lidar and balloon soundings in clear conditions over Athens, that mixed layer heights during the 84% partial eclipse were reduced from 800 m to 620 m.

For the 20 March 2015 eclipse there is observational evidence of the depth of the boundary layer available from a radiosonde ascent launched from Reading (51.44°N, 0.94°W) before eclipse onset (0848 UTC) which landed in Winchester (31 miles southwest) at 1013 UTC, and from a UHF Doppler radar wind profiler operating at Cardington (52.10°N,0.42°W, [30]) throughout the eclipse event (neither sets of data are shown). The boundary depth, inferred from the height of the temperature inversion, decreases during the morning in the vicinity of Reading, but this decrease is not inconsistent with the synoptic evolution expected from model profiles. In contrast, at Cardington there is evidence from the wind profiler of a slow reduction in boundary layer depth throughout the morning (from about 900 m at 0300 UTC, to about 600 m at 0800 UT, and then to 500 m at 1000 UTC) before the boundary layer deepens again after noon. Thus, the boundary layer is shallowest at about the time of the maximum eclipse. While this boundary depth reduction cannot be confidently attributed to the eclipse, a similar decrease in boundary layer depth is not observed in hourly model profiles (again from a model ignorant of the eclipse) taken at Cardington. Ref. [31] provides other evidence of boundary layer changes during this eclipse through observations showing a reduction in cloud base height of 20 m during the passage of the eclipse, together with other boundary layer changes in temperature and wind speed consistent with findings from the wider observation network analysed in this paper. Comparison of the operational weather forecasts made by the Met Office UKV model against a forecast made by the same model but including a parametrization for the eclipse in the model code shows shallower boundary layer depths in the clear sky region, and in Scotland and Northern Ireland, in the forecast from the model with the eclipse parametrization at the time of the maximum eclipse [32]. These model results reveal that a boundary layer depth change attributable to the eclipse would be expected to have occurred at Cardington but not at Reading, consistent with the available observations described above.

Effects of boundary layer depth changes can be represented by a theoretical model of the boundary layer such as that of [26]. This model relates the surface drag coefficient, C_D, and boundary height, h, with the northwards, u, and westwards, v, components of the wind speed

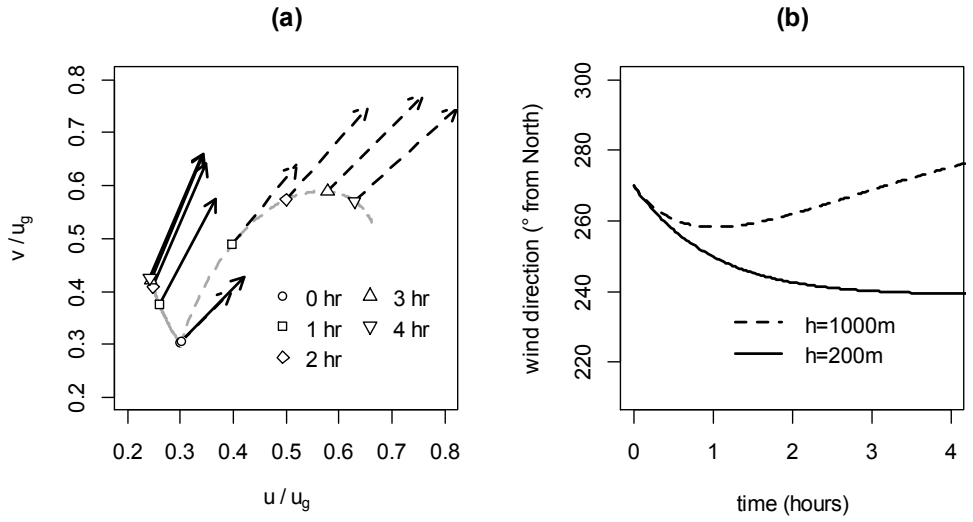

Figure 14. Illustrative calculations of the variation in wind direction for atmospheric boundary layer heights of 1000 m (dashed lines) and 200 m (solid lines), using the theoretical model of ref. [26]. (a) Hodograph showing the wind vectors at hourly intervals, beginning from initial wind vector components u and v of 3 ms^{-1} (at $t = 0$). The values of u and v have been normalised by an assumed geostrophic wind speed u_g of 10 ms^{-1}. (b) Time series of the calculated wind directions for the two boundary layer heights. (Drag coefficient $C_D = 8 \times 10^{-3}$, and Coriolis parameter calculated for 50°N.)

by two coupled equations:

$$\begin{aligned} \frac{du}{dt} - fv &= -C_D\sqrt{u^2+v^2}\left(\frac{u}{h}\right), \\ \frac{dv}{dt} - f(u-u_g) &= -C_D\sqrt{u^2+v^2}\left(\frac{v}{h}\right), \end{aligned}$$

where f is the Coriolis parameter, and u_g is the free geostrophic wind speed above the layer. These coupled time-dependent ordinary differential equations can be solved numerically for u and v as a function of time t, if representative values of C_D and h are assumed, given initial conditions for u and v at $t = 0$.

Figure 14(a) shows time-dependent numerical solutions (i.e. the variations of u and v with time t) calculated for two different layer depths, beginning with initial values of u and v (at $t = 0$) chosen to approximate the wind speeds in the Midlands regions around the eclipse time. (A fourth order adaptive Runge-Kutta numerical method was used for these calculations, from [33].) In Fig. 14(a) the magnitudes of the wind vectors at hourly intervals found by integration from the initial values are plotted against each other in hodograph form, to show the associated changes in direction with time. The two boundary layer heights were selected to give an illustrative comparison between the situations of sustaining an established boundary layer in clear skies, and the much shallower boundary layer which may be formed during an eclipse. With time, the wind direction in the shallow boundary layer case turns anticlockwise, compared with the more constant wind direction maintained in the deeper boundary layer case. Fig. 14(b) shows the continuous variation in wind directions against time (from which the sampled hourly values of Fig. 14(a) were obtained.) Although the exact surface and flow parameters of the regions are not attempted to be represented, the wind direction change apparent under these assumptions is not inconsistent with that observed in Figs. 12(c,d). Similar nocturnal oscillatory behaviour has been observed in near surface winds from the Cabauw observatory [23].

6. Conclusions

In addition to the well-documented cooling, increase in RH and slackening of the near-surface wind speed, wind direction changes can also be attributed to an eclipse. While confidence in wind speed changes is similar to that in temperature and RH, these far exceed confidence in the wind direction changes. Nevertheless the wind direction changes remain of broader interest, because of their relationship to the supposed "eclipse wind". It is noteworthy that the wind direction changes have been found to be robust across the two eclipse events in 1999 and 2015, with the latter analysis here using two independent observation networks. Some theoretical support for the wind direction changes identified in the clear sky inland regions is provided by considering the rapid eclipse-induced cooling as analogous to the formation of nocturnal wind structures. This may provide a more parsimonious explanation for the surface wind direction changes observed than the substantial mesoscale structure postulated by [11].

Finally, a spatially dense, high temporal resolution (subhourly) meteorological observation network is invaluable for studies of meteorological responses to transient phenomena. The roadside network here employed now provides a further novel valuable source of such meteorological measurements.

Data accessibility. The hourly weather observations MIDAS dataset and operational output from the MetUM is available through the British Atmospheric Data Centre (BADC). The data files for the Vaisala roadside network and one-minute Met Office surface station wind measurements were obtained directly from Vaisala and the Met Office, respectively.

Acknowledgements. The authors thank David Bullock from Vaisala for his extraction of and provision of data from the roadside network of stations. Whitney Nobbs undertook an important preliminary study of the roadside network data available. The Met Office is thanked for making the operational weather forecast data and MIDAS dataset available through BADC. Matthew Clark from the Met Office kindly provided the one-minute MIDAS wind data. Janet Barlow (University of Reading) provided very helpful ideas that led to the nocturnal jet formation mechanism being discussed here. We thank the National Centre for Atmospheric Science (NCAS) for provision of the Cardington wind profiler data and Emily Norton from the NCAS Atmospheric Measurement Facility in particular for kindly producing plots for us of the Cardington wind profiler observations.

Conflict of interests. We have no competing interests

Authors' contributions. SLG extracted and analysed the observational and model data and drafted the manuscript. RGH and SLG both designed the study. RGH provided some analysis code, performed the analysis of the nocturnal jet, assisted in the interpretation of the analysis and edited the manuscript.

References

1. Sjöblom A. 2010. A solar eclipse seen from the High Arctic during the period of midnight sun: effects on the local meteorology. *Meteorology and Atmospheric Physics*, **107**, 123-136. (doi:10.1007/s00703-010-0070-3)
2. Aplin KL, Scott CJ and Gray SL. 2016. Atmospheric changes from solar eclipses. *This volume*
3. Murthy BS, Latha R, Sreeja P and Dharmaraj T. 2012. Transient land breeze: Eclipse induced wind flow modifications—Observations over plant canopy, *J. Atmos. Sol.-Terr.* **89**, 33-39, (doi:10.1016/j.jastp.2012.07.010).
4. Bhat GS and Jagannathan R. 2012. Moisture depletion in the surface layer in response to an annular solar eclipse. *J. Atmos. Sol.-Terr.* **80**, 60-67. (doi: 10.1016/j.jastp.2012.02.025)
5. Namboodiri KVS, Dileep PK, Mammen K, Ramkumar G, KiranKumar NVP, Sreenivasan S, Kumar BS and Manchanda RK. 2011. Effects of annular solar eclipse of 15 January 2010 on meteorological parameters in the 0 to 65 km region over Thumba, India. *Meteorol. Z.* **20**, 635-647. (doi:10.1127/0941-2948/2011/0253)
6. Founda D, Melas D, Lykoudis S, Lisaridis I, Gerasopoulos E, Kouvarakis G, Petrakis M and Zerefos C. 2007. The effect of the total solar eclipse of 29 March 2006 on meteorological variables in Greece. *Atmos. Chem. Phys.* **7**, 5543-5553.

7. Winkler P, Kaminski U, Köhler U, Riedl J, Schroers H and Anwender D. 2001. Development of meteorological parameters and total ozone during the total solar eclipse of August 11, 1999. *Meteorol. Z.* **10**, 193-199.
8. Eaton D, Hines JR, Hatch WH, Cionco RM, Byers J, Garvey D and Miller DR. 1997. Solar eclipse effects observed in the planetary boundary layer over a desert. *Bound. Layer Meteorol.*, **83**, 331-346.
9. Nymphas EF, Adeniyi MO, Ayoola MA and Oladiran EO. 2009. Micrometeorological measurements in Nigeria during the total solar eclipse of 29 March. *J. Atmos. Sol.-Terr.* **71**, 1245-1253. (doi:10.1016./j.jastp.2009.04.014).
10. Clayton HH. 1908. The Meteorology of Total Solar Eclipses, Including the Eclipse of 1905. *Annals of Harvard College Observatory*, **58**. 192-216.
11. Clayton HH. 1901. The eclipse cyclone and the diurnal cyclones. *Ann. Astron. Observ. Harvard College.* **43**, 5-22.
12. Bigelow FH. 1901. Clayton's eclipse cyclone and the diurnal cyclones. *Science*, **13**, 589-591.
13. Clayton HH. 1901. Clayton's eclipse cyclone and the diurnal cyclones. *Science*, **13**, 747-750.
14. Gray SL and Harrison RG. 2012. Diagnosing eclipse-induced wind changes. *Proc. R. Soc. A.* **468**, 1839-1850. (doi:10.1098/rspa.2012.0007)
15. Aplin KL and Harrison RG 2003. Meteorological effects of the eclipse of 11 August 1999 in cloudy and clear conditions. *Proc. R. Soc. A.* **459**, 353-371. (doi:10.1098/rspa.2002.1042)
16. Prenosil T. 2000. The influence of the 11 August 1999 solar eclipse on the weather over Central Europe. *Meteorol. Z.* **9**. 351-359.
17. KiranKumar NVP, Purushothaman N and Santosh M. 2013. Response of spectral characteristics of wind and temperature of atmospheric surface layer to the noontime annular solar eclipse. *J. Atmos. Sol.-Terr.* **97**, 91-98. (doi:10.1016/j.jastp.2013.02.017)
18. Met Office. 2006. UK Hourly Weather Observation Data, Part of the Met Office Integrated Data Archive System (MIDAS). NCAS British Atmospheric Data Centre, 2 February 2016. (http://catalogue.ceda.ac.uk/uuid/916ac4bbc46f7685ae9a5e10451bae7c)
19. Vaisala Road Weather Station RWS200. (See http://www.vaisala.com/en/roads/products/roadweathersystems/Pages/RWS200.aspx), Accessed: 21 October 2015.
20. Davies T, Cullen MJP, Malcolm AJ, Mawson MH, Staniforth A, White AAand Wood N. 2005. A new dynamical core for the Met Office's global and regional modelling of the atmosphere. *Q. J. R. Meteorol. Soc.* **131**, 1759-1782. (doi:10.1256/qj.04.101)
21. Tang Y, Lean HW and Bornemann J. 2013. The benefits of the Met Office variable resolution NWP model for forecasting convection. *Meteorol. Appl.*, **20**, 417-427. (doi:10.1002/met.1300)
22. Harrison RG. 2014. *Meteorological measurements and instrumentation.* pp280. Wiley-Blackwell.
23. Baas P, van de Wiel BJH, van den Brink L and Holtslag AAM. 2012. Composite hodographs and inertial oscillations in the nocturnal boundary layer, *Quart. J. Roy. Meteorol. Soc.*, **138**, 528–535. (doi.org/10.1002/qj.941)
24. Barlow JF, Halios CH, Lane SE and Wood CR. 2014. Observations of urban boundary layer structure during a strong urban heat island event, *Environmental Fluid Mechanics*, **15**, 373–398. (doi.org/10.1007/s10652-014-9335-6)
25. Blackadar AK. 1957. Boundary layer wind maxima and their significance for the growth of the nocturnal inversion. *Bull. Am. Meteorol. Soc.*, **38**, 283-290.
26. Thorpe AJ and Guymer TH. 1977. The nocturnal jet. *Quart. J. Roy. Meteorol. Soc.*, **103**, 633-653.
27. Wingo SM and Knupp KR. 2015. Multi-platform Observations Characterizing the Afternoon-to-Evening Transition of the Planetary Boundary Layer in Northern Alabama, USA. *Boundary Layer Meteorol.*, **155**, 29-53. (doi:10.1007/s10546-014-9988-1).
28. Girard-Ardhuin F, Bénech B, Campistron B, Dessens J and Jacoby-Koaly S. 2003. Remote Sensing and surface observations of the response of the Atmospheric Boundary Layer to a Solar Eclipse. *Boundary Layer Meteorol.*, **106**, 93-115. (doi:10.1023/A:1020837400800)
29. Amiridis V, Melas D, Balis DS, Papayannis A, Founda D, Katragkou E, Giannakaki E, Mamouri RE, Gerasopoulos E and Zerefos C. 2007. Aerosol Lidar observations and model calculations of the Planetary Boundary Layer evolution over Greece, during the March 2006 Total Solar Eclipse. *Atmos. Chem. Phys.*, **7**, 6181-6189. (doi:10.5194/acp-7-6181-2007
30. Norton EG. 2015. Vertical wind profile data from 6th November 2013 to present measured by the University of Manchester 1290 mhz mobile wind profiler deployed on long term observations at Met Office Research Unit,

Cardington, Bedfordshire. NCAS British Atmospheric Data Centre, 11 March 2016. (http://catalogue.ceda.ac.uk/uuid/ecbecb0fbf6e4a4e93bb3ee2cf9854cd)
31. Burt S. 2016. Meteorological responses in the atmospheric boundary layer over southern England to the deep partial eclipse of 20 March 2015. *This volume*
32. Clark PA. 2015. Numerical forecasts of the impact of the 20 March 2015 eclipse on UK weather. *This volume*
33. Press WH, Flannery BP, Teukolsky SA and Vetterling WT. 1989. *Numerical recipes in Pascal*. Cambridge UK: Cambridge University Press.